

Coherent Quantum Oscillations in a Silicon Charge Qubit

Zhan Shi,¹ C. B. Simmons,¹ D. R. Ward,¹ J. R. Prance,¹ Teck Seng Koh,¹ John King Gamble,¹ X. Wu,¹ D. E. Savage,¹ M. G. Lagally,¹ Mark Friesen,¹ S. N. Coppersmith,¹ and M. A. Eriksson¹

¹*University of Wisconsin-Madison, Madison, WI 53706*

We report coherent oscillations in a charge qubit formed in a top-gated Si/SiGe double quantum dot. We observe Rabi oscillations (x -rotations on the Bloch sphere) between the (2,1) and (1,2) charge states, with a figure of merit (number of oscillations per T_2^* coherence time) of 10 at the charge degeneracy point, where T_2^* is 2.1 ns. Unlike previous measurements of charge qubits in quantum dots, the longest T_2^* of 3.7 ns is found away from the charge degeneracy point; this feature arises from an anticrossing between the (2,1) ground state and a (1,2) excited state, indicating that internal structure of the quantum dots can be used to enhance coherence. In this regime we find a figure of merit of 37. We also observe Ramsey fringes (z -rotations on the Bloch sphere) and use them to extract a T_2^* of 179 ps at detunings away from any protective energy level structure.

Fast, coherent oscillations can be performed using qubits based on charge, as demonstrated in superconducting circuits [1, 2] and semiconductor quantum dots [3, 4]. Charge states, however, have relatively fast decoherence [4, 5]. Spin qubits offer much longer coherence, and spins in silicon-based structures have especially long spin coherence times, because of the predominance of spin-zero nuclear isotopes and relatively weak spin-orbit coupling [6–8]. Recent experiments have demonstrated coherent quantum oscillations of singlet-triplet spin qubits in Si/SiGe [9] with substantially longer intrinsic spin T_2^* times than singlet-triplet qubits in GaAs heterostructures [10–12]. However, because fast manipulation of semiconductor spin qubits relies on transient mixing of spin degrees of freedom with charge degrees of freedom (either through spin-orbit coupling [13] or the exchange interaction [14]), charge coherence determines the ultimate fidelity of spin qubits [14–19]. Methods to extend charge coherence will enhance the ability to perform high fidelity manipulation of spin qubits.

Here, we demonstrate coherent control and measure the rates of dephasing of fast oscillations of a charge qubit in a Si/SiGe double quantum dot between the (2,1) and (1,2) charge states. Rabi oscillations with a figure of merit (number of oscillations per T_2^* time) of 10 are measured at the charge degeneracy point, where the decay time T_2^* of the oscillations is 2.1 ns. In sharp contrast to previous measurements of charge qubits [1–5], we find an enhanced T_2^* away from the charge degeneracy point, which we show arises because of the internal structure of the right quantum dot. A low-lying excited state of the (1,2) charge configuration anticrosses with the (2,1) ground state, leading both to quantum interference between the (1,2) ground and excited states and to oscillations in the state of the charge qubit. In this regime we find $T_2^* = 3.7$ ns and a figure of merit of 37. To probe oscillations about an orthogonal axis on the Bloch sphere we use a two-pulse sequence to observe Ramsey fringes. Away from any protective energy level structure the Ramsey fringes reveal a charge T_2^* time of 179 ps.

A scanning electron microscope image of a device identical to the one measured in the experiment is shown in Fig. 1(a). The double quantum dot used here was fabricated in a Si/SiGe heterostructure as described in Refs. [20, 21]. Changes in the charge states of the left and right dots are observed through measurements of the current I_{QPC} through the nearby charge sensing quantum point contact (QPC), as shown in Fig. 1(a). The stability diagram in Fig. 1(b) shows the QPC transconductance $G_L = \partial I_{\text{QPC}} / \partial V_L$, measured using a lock-in amplifier, as a function of the voltages on gates L and PR. Using magnetospectroscopy [22], we have determined that the white polarization line is where the effective charge state of the double dot changes between (2,1) and (1,2).

Near the charge degeneracy point, at which the energies of the (2,1) and (1,2) states are equal, the system is well-described by the Hamiltonian of a two-state system:

$$H = \begin{pmatrix} \varepsilon/2 & \Delta \\ \Delta & -\varepsilon/2 \end{pmatrix}, \quad (1)$$

where Δ is the tunnel coupling between the two states and ε is the detuning, the energy difference between the two states in the absence of tunnel coupling. Coherent oscillations between the two charge states can be observed when the detuning ε is changed abruptly. For example, just after the detuning is increased suddenly from a large negative value to $\varepsilon = 0$, as shown in Fig. 1(e), the system Hamiltonian $H = \Delta \sigma_x$, with the initial wavefunction being a position eigenstate. Subsequently, the system oscillates between the two position eigenstates at the Rabi angular frequency $2\Delta/\hbar$. More generally, suddenly increasing the detuning ε to a larger value ε' induces oscillations at the angular frequency $\Omega_R = \sqrt{\varepsilon'^2 + 4\Delta^2}/\hbar$; as one moves away from the polarization line, the oscillations increase in frequency and decrease in amplitude.

To observe Rabi oscillations, the tunnel coupling between the quantum dots must be tuned appropriately, which we do by changing the voltage on gate T until the polarization line is broadened slightly more than the electron temperature, which we have measured to be

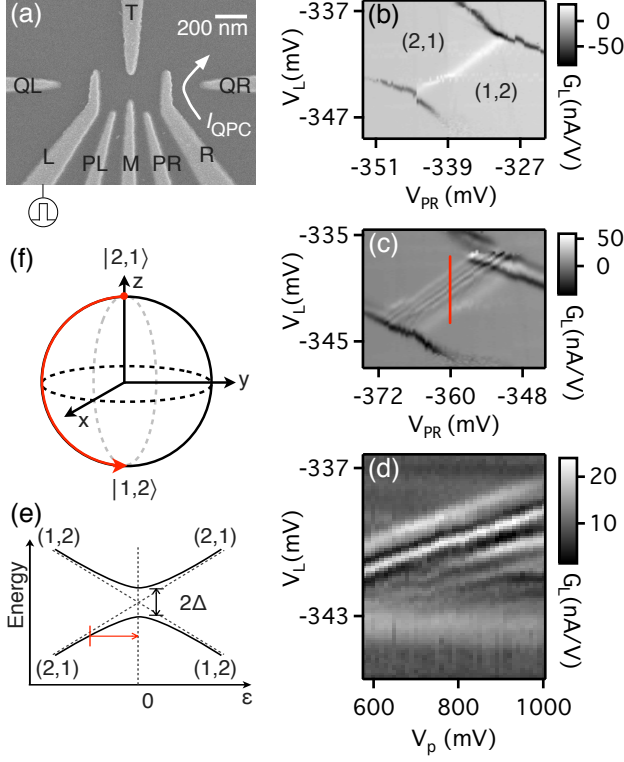


FIG. 1. (a) SEM image of a device identical to the one used in the experiment. The charge state of the double dot was determined by measuring the current through the quantum point contact (QPC). Voltage pulses are applied to gate L. (b) Stability diagram of the double dot with effective charge occupations labeled. The transconductance $G_L = \partial I_{\text{QPC}} / \partial V_L$ is shown as a function of the two gate voltages V_L and V_{PR} ; the lines in the diagram correspond to changes in the double dot charge occupation. The polarization line is white, and corresponds to a change in the effective electron occupation from (2,1) to (1,2). (c) Stability diagram in the presence of a pulsed voltage applied to gate L. (d) Charge resonance positions as a function of pulse amplitude. As expected for Rabi oscillations, the displacement in V_L of the peaks from the polarization line increases as the pulse amplitude V_P increases. (e) Diagram of energy levels versus detuning, showing the expected anticrossing of the (2,1) – (1,2) charge transition. The red arrow shows the effect of an applied voltage pulse with the dc detuning and pulse amplitude chosen to place the peak of the pulse at $\varepsilon = 0$. (f) Bloch sphere of the charge qubit. The red arrow indicates a π -rotation about the x -axis.

$T_e = 143 \pm 10$ mK [21]. This value corresponds to a tunnel rate ≥ 3 GHz [23], a quantity we measure more precisely below based on the observed Rabi oscillation frequency. As indicated schematically in Fig. 1(a), pulsed voltages are applied to gate L through a bias tee using a commercial pulse generator (Agilent 81134A). Fig. 1(c) shows the measured stability diagram in the presence of a 580 mV pulse (which after attenuation in the coax path is calibrated to be 3.82 mV on gate L) of duration 500 ps applied at a repetition rate of 40 MHz. A series of reso-

nances parallel to the polarization line are clearly visible, corresponding to partial time-averaged occupation of the (1,2) charge state in the region in which the (2,1) charge state is the ground state. Fig. 1(d) shows a measurement of G_L along the red line in Fig. 1(c) in the presence of a voltage pulse of width 375 ps with varying amplitude V_P . The positions of the resonances visible in Fig. 1(c) shift linearly with pulse amplitude, providing evidence that the oscillations result from pulsing the (2,1) charge state non-adiabatically into the vicinity of the charge-state anticrossing. Both the angle and the rate of rotation on the Bloch sphere (Fig. 1(f)) depend on the proximity of the pulse peak to the charge anticrossing, which varies as a function of V_L , resulting in oscillations in the measured G_L .

Figure 2(a) shows Rabi oscillations between the (2,1) and (1,2) charge states: the transconductance G_L is plotted as a function of the duration of the pulse and of the voltage V_L , which determines the distance of the detuning from the polarization line. Oscillations of the signal are apparent out to several nanoseconds, and the oscillation frequency is faster towards the bottom of Fig. 2(a), where the detuning ε at which the Rabi precession is occurring is largest. The coherence time is longest when the oscillations are fastest, with more than 40 well-defined oscillations present in Fig. 2(a).

To characterize the oscillations quantitatively, we integrate the data presented in Fig. 2(a) from top to bottom to calculate the total change in dot charge, calibrated by using the fact that the total charge transferred across the polarization line is one electron, and we smooth by averaging over three adjacent pixels. The vertical axis is converted to ε_p , the detuning value at the peak of the pulse, by noting that the main, slowest oscillation corresponds to $\varepsilon_p = 0$, and by fitting the change in frequency as a function of V_L for small positive ε_p . Fig. 2(c–e) present the resulting gray-scale images; Fig. 2(g–i) show line cuts through the corresponding plots, revealing clear oscillations of the average charge as a function of time. By fitting the amplitude of these oscillations to exponential decays, we extract a dephasing time T_2^* of 2.1 ± 0.4 ns at $\varepsilon_p = 0$ and, intriguingly, of 3.7 ± 0.6 ns when $\varepsilon_p = 59 \mu\text{eV}$. This increase in coherence time for $\varepsilon > 0$ yields a T_2^* that is substantially longer than the value of ~ 0.3 ns measured by Petersson *et al.* [4] in a GaAs charge qubit far away from its charge degeneracy point. We return to a discussion of this increase below.

We now demonstrate coherent rotations of the qubit about the z -axis of the Bloch sphere by performing a Ramsey fringe experiment [24, 25] using the procedure illustrated in Fig. 3(a). First, a pulse is applied that rotates the Bloch vector around the x -axis by an angle $5\pi/2$, rotating it from being along z to along y (we use a $5\pi/2$ pulse of amplitude 400 mV and duration 300 ps instead of a $\pi/2$ pulse because of the difficulty of creating high-quality pulses as short as 60 ps). After a variable

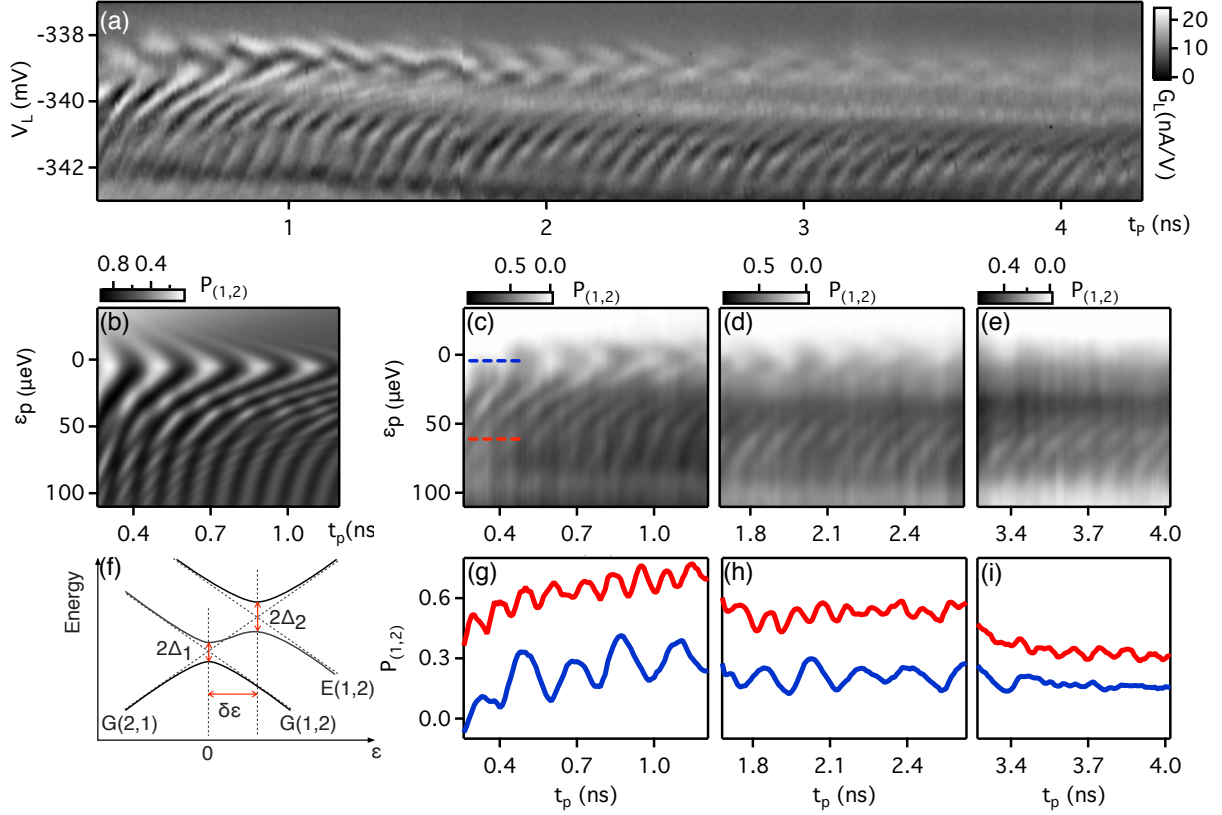


FIG. 2. (a) Differential conductance G_L of the charge-sensing quantum point contact as a function of pulse duration t_p and gate voltage V_L for pulses of amplitude $V_p = 800$ mV (5.27 mV on gate L). The signal oscillates as the duration of the pulses is increased, with a frequency that is a minimum when the pulse takes the state of the system to the polarization line (detuning $\varepsilon = 0$). The decoherence time T_2^* that governs the decay of the oscillations is longer at larger detunings. (b) Simulation of the Rabi oscillations as described in the main text. (c-e) Integration of the differential conductance shown in (a) yields the average charge state of the dot as a function of ε_p , as described in the text. The Rabi oscillations arising from the anticrossing of the (2,1) and (1,2) ground states is clearly visible at $\varepsilon_p = 0$. The data are acquired as a series of vertical sweeps, and in panels (c-e) each such sweep is offset to compensate for the increasing pulse duration with increasing t_p , so that the reference voltage V_L and thus ε_p is independent of t_p . The data in all three subpanels are smoothed by averaging over three diagonally adjacent pixels. (f) Energy level diagram showing two nearby anticrossings, as described in the main text. (g-i) Line cuts at two values of V_L indicated by the red and blue dashed lines in (c). The Rabi frequency is larger at larger detuning, as expected. The coherence time governing the decay of the oscillations is longer at nonzero detuning than when the detuning is zero. Because the Rabi frequency and the coherence time both increase as the detuning is increased, the number of observed oscillations is largest at large detuning, with 42 oscillations clearly apparent in (a).

time, during which the system evolves at the base value of the detuning, a second pulse is applied that rotates the state about the x -axis on the Bloch sphere by $5\pi/2$. The charge measured at the end of this process oscillates as a function of the time between the two $5\pi/2$ pulses at a frequency $f = \sqrt{\varepsilon^2 + 4\Delta^2}/h$, where ε is the detuning in the absence of the pulse. Fig. 3(b) shows the differential conductance G_L measured through the charge sensor for a pulse amplitude of 400 mV (2.64 mV on gate L) as a function of the gate voltage V_L and τ , the time between the start of the first and second $5\pi/2$ pulses, with a repetition rate of 40 MHz. For very short τ , the $5\pi/2$ pulses overlap and one is essentially performing a Rabi oscillation experiment. At $\tau \gtrsim 300$ ps (red dashed

box in Fig. 3(c)) the time interval between the end of the first $5\pi/2$ pulse and the start of the second becomes nonzero, and the oscillations that are observed reflect the rotation of the Bloch vector between the two pulses. We have verified that the temporal period of the Ramsey fringes decreases if we decrease the detuning at which the Ramsey precession occurs (data not shown). To analyze these data quantitatively, we again integrate the differential conductance and normalize by noting that the total charge transferred across the polarization line is one electron (Fig. 3(c)). Fig. 3(d) shows a cut through the integrated data at the value of V_L marked by the blue arrow. After subtraction of a smooth background (smooth gray curve in Fig. 3(d)), the resulting oscillating curve is fit

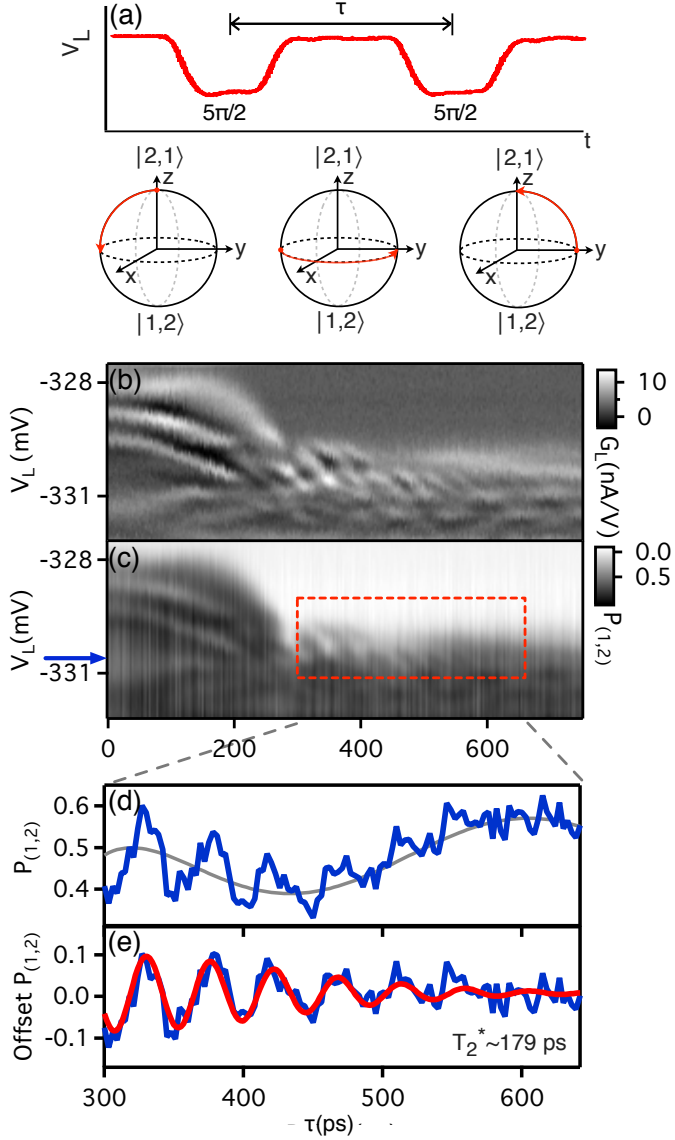


FIG. 3. (a) Schematic of the Ramsey fringe experiment that demonstrates coherent control of oscillations about the z -axis of the Bloch sphere. A $5\pi/2$ pulse of duration 300 ps is applied to rotate the qubit Bloch vector around the x -axis into the $x-y$ plane. The system then evolves for a variable time τ , and a second $5\pi/2$ pulse is then applied. The oscillations observed as a function of the time between pulses reflect the rotation of the Bloch vector in the $x-y$ plane. (b) Differential conductance through the QPC as a function of the gate voltage V_L and of the pulse delay τ . The two pulses overlap for $\tau < 300$ ps; oscillations are observed for $\tau > 300$ ps, corresponding to Ramsey fringes arising from the rotation of the state about the z -axis of the Bloch sphere. (c) Integrated transconductance, normalized by noting that the total charge transferred across the polarization line is one electron. Red dashed box shows the location of the Ramsey fringes. (d) Blue: Line cut of the data in (c) at the detuning marked by the blue arrow. Gray: Smooth background that is subtracted from the line cut before fitting the data to a damped sinusoidal form. (e) Blue: data from (d) with background subtracted. Red: fit to the form $A \exp(-(t - t_0)^2/T_2^{*2}) \cos(\omega t + \phi) + C$, which yields a value for the decoherence time T_2^* of 179 ps.

to the product of a cosine function and a Gaussian. This procedure yields $T_2^* = 179 \pm 18$ ps, substantially longer than the value of 60 ps obtained by measuring Ramsey fringes for a GaAs charge qubit and using a similar fitting procedure [25]. Calculations following the methods of Ref. [26] show that the charge dephasing rate in GaAs from polar optical phonons is of order 1 GHz, whereas similar calculations for phonon-induced charge dephasing in Si yield values of order 0.5 MHz. Thus, in both materials, and particularly in Si, improvements may be possible through a reduction of excess charge noise.

We now return to the increase in the coherence time T_2^* of the Rabi oscillations for $\varepsilon_p > 0$. This behavior is in sharp contrast to the results that have been obtained for charge qubits in GaAs semiconductor quantum dots and in superconducting charge qubits [4, 5]. Moreover, such an increase in T_2^* with increasing ε_p is generally unexpected, because the qubit is well protected from charge noise — that is, from environmental noise in the detuning ε — at the “sweet spot” corresponding to $\varepsilon_p = 0$. The data of Fig. 2(c-e) contain an important clue to the origin of this behavior: the Rabi oscillations at larger detuning are faster than those near $\varepsilon_p = 0$, yet the increase in Rabi frequency seems to saturate at about $\varepsilon_p = 50$ μ eV. In fact, the Rabi oscillations appear as an approximately parallel series of lines from $\varepsilon_p = 50$ to 100 μ eV.

The long-lived Rabi oscillations at large ε_p can be explained by the presence of an anticrossing between the $(2,1)$ ground state $G(2,1)$ and the $(1,2)$ excited state $E(1,2)$, as shown in Fig. 2(f). The effect of this second anticrossing is shown in the theoretical simulation plotted in Fig. 2(b), which makes use of the following parameters (as defined in the figure): tunneling amplitude $\Delta_1 = 11.2$ μ eV (determined directly from the Rabi oscillation period at $\varepsilon = 0$), tunneling amplitude $\Delta_2 = 14.5$ μ eV, detuning difference $\delta\varepsilon = 45$ μ eV, and a voltage pulse rise time of 80 ps (from the specifications of the Agilent 81134A pulse generator). Dephasing is incorporated phenomenologically as described in Ref. [26]; additional details about the simulations and the choice of parameters are in the supplementary material.

The second anticrossing has two effects. First, Rabi oscillations at the anticrossing between $G(2,1)$ and $E(1,2)$ lead to small distortions in both the measured and simulated oscillation patterns at small, positive ε_p ; these are easily visible in the simulation shown in Fig. 2(b) and can be found in the data at the right side of Fig. 2(c). More importantly, because the inverse rise time of the pulse is comparable to Δ_1 and Δ_2 , for large ε_p the voltage pulse takes the state $G(2,1)$ into a superposition of $G(1,2)$ and $E(1,2)$ — that is, the transition through the two anticrossings is not fully abrupt. These two states $G(1,2)$ and $E(1,2)$ accumulate phase at different rates, leading to oscillations at the frequency $f_{GE} = 2\delta\varepsilon/h$. Thus, the long-lived coherent oscillations at large ε_p — the parallel lines in Fig. 2(c-e) the range $\varepsilon_p = 50$ to 100 μ eV — arise

from the interference between states $G(1,2)$ and $E(1,2)$. The energies of these states have the same dependence on ε , providing protection from charge noise that is similar (but even better than) the protection that occurs near an energy level anticrossing [18, 27].

The existence of the low-lying excited state $E(1,2)$ is consistent with magnetospectroscopy measurements showing that the right dot has a very small or negative singlet-triplet splitting in the two-electron state (data not shown). In contrast, the first excited state of the left dot is large in energy (approximately $200 \mu\text{eV}$) [22] and therefore can be neglected. This energy level spectrum also is consistent with the much shorter T_2^* for the Ramsey fringes of Fig. 3(e). Because of the large energy gap to the $(2,1)$ first excited state, there is no additional anticrossing in the experimental range $\varepsilon < 0$. As shown in Fig. 2(f), the energy gap driving the Ramsey interference is thus directly proportional to ε and to charge noise induced fluctuations in that quantity. It is thus natural that the T_2^* extracted from the Ramsey fringe data of Fig. 3 should be shorter than that derived from the Rabi oscillation data of Fig. 2: the Ramsey fringes arise from precession of the Bloch vector at a detuning where the energy gap is very sensitive to charge fluctuations.

In summary, we have observed coherent quantum charge oscillations in a qubit formed in a Si/SiGe double quantum dot. Both Rabi oscillations and Ramsey fringes are observed. The coherence time T_2^* for Rabi oscillations is maximum away from the charge degeneracy point, because of the existence of a low-lying excited state in the right-hand quantum dot, demonstrating that the internal structure of quantum dots can be exploited to enhance coherence.

This research was supported in part by the U.S. Army Research Office (W911NF-08-1-0482), the NSF (DMR-0805045), and by the United States Department of Defense. The views and conclusions contained in this document are those of the authors and should not be interpreted as representing the official policies, either expressly or implied, of the US Government. This research utilized NSF-supported shared facilities at the University of Wisconsin-Madison.

SUPPLEMENTARY INFORMATION

We model the dynamical evolution of the density matrix ρ of the three electron, double quantum dot system by a master equation [28, 29]

$$\dot{\rho} = -\frac{i}{\hbar}[H, \rho] + D, \quad (2)$$

where H is the three-state Hamiltonian and D is a phenomenological term that describes pure dephasing of the charge state under the assumption of Markovian dynamics, as appropriate for the double dot system. H and D

are given, in the $\{|a\rangle \equiv |G(2,1)\rangle, |b\rangle \equiv |G(1,2)\rangle, |c\rangle \equiv |E(1,2)\rangle\}$ basis, by

$$H = \begin{pmatrix} \varepsilon/2 & \Delta_1 & \Delta_2 \\ \Delta_1 & -\varepsilon/2 & 0 \\ \Delta_2 & 0 & \delta\varepsilon - \varepsilon/2 \end{pmatrix}, \quad (3)$$

$$D = - \begin{pmatrix} 0 & \Gamma_{ab} \rho_{ab} & \Gamma_{ac} \rho_{ac} \\ \Gamma_{ab} \rho_{ba} & 0 & 0 \\ \Gamma_{ac} \rho_{ca} & 0 & 0 \end{pmatrix}, \quad (4)$$

where Δ_1 and Δ_2 are tunnel coupling matrix elements, ε is the detuning, $\delta\varepsilon$ is the energy separation of the ground and excited $(1,2)$ states ($|b\rangle$ and $|c\rangle$), and Γ_{ab} and Γ_{ac} are dephasing rates ($1/T_2^*$) that describe the exponential decay of the coherences between different charge states of the qubit, presumably caused by charge noise.

From the data, the dephasing rates show a dependence on detuning. Dephasing rates increase away from a minimum of $\Gamma_i = 0.48 \text{ GHz}$ at detuning $\varepsilon = 0$, corresponding to the position of the first anticrossing. Similar behavior of noise in the detuning parameter has been observed in GaAs double dot charge qubits with one anticrossing [3, 4].

We use the T_2^* value of 179 ps at a detuning of $-63 \mu\text{eV}$ derived from the Ramsey experiment, combined with the intrinsic minimum observed in the Rabi oscillations to model the dephasing rates. They are given as a quadrature sum of the intrinsic rate Γ_i and a detuning dependent rate $\alpha\Gamma_\varepsilon$:

$$\Gamma_{ab} = \sqrt{\Gamma_i^2 + (\alpha_{ab} \Gamma_\varepsilon)^2}, \quad (5)$$

$$\Gamma_{ac} = \sqrt{\Gamma_i^2 + (\alpha_{ac} \Gamma_\varepsilon)^2}, \quad (6)$$

where Γ_ε is a parameter that is determined by experimental values of T_2^* at two values of detuning as described above. The variables α_{ab} and α_{ac} play the role of describing the relative fluctuations in energy between different charge states due to changes in detuning. In terms of the slopes of energy versus detuning, they are

$$\alpha_{ab}(\varepsilon_j) \equiv \left| \frac{dE_a}{d\varepsilon} - \frac{dE_b}{d\varepsilon} \right|_{\varepsilon=\varepsilon_j}, \quad (7)$$

$$\alpha_{ac}(\varepsilon_j) \equiv \left| \frac{dE_a}{d\varepsilon} - \frac{dE_c}{d\varepsilon} \right|_{\varepsilon=\varepsilon_j}. \quad (8)$$

Eqs. 5 and 6 produce dephasing that decreases as the relative slopes of a pair of energy-detuning curves gets flatter, and vice versa, as observed in the data.

Electrical pulses applied to gate L control the detuning ε as a function of time, and this is modeled as a smooth trapezoid with a rise time of 80 ps (from the specifications for the Agilent 81134A pulse generator) and pulse amplitude of $127 \mu\text{eV}$.

The tunable parameters that go into our simulation are the values of the tunnel couplings Δ_1 and Δ_2 , and the energy separation $\delta\varepsilon$ between the ground and excited $(1,2)$

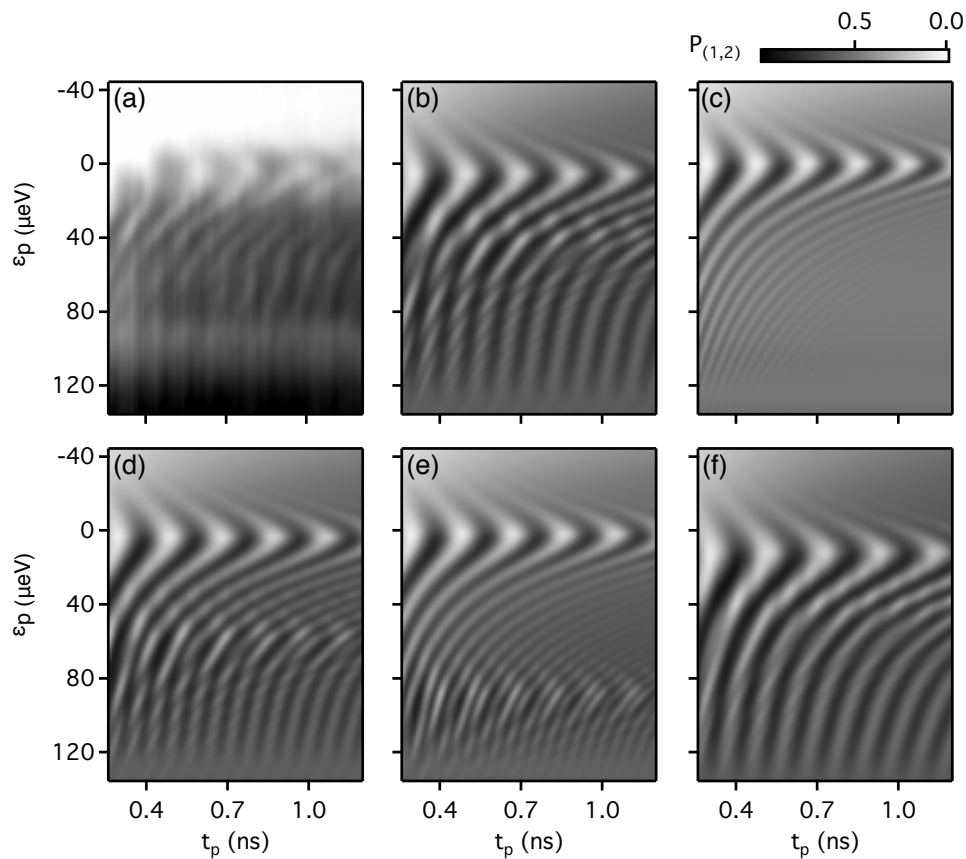


FIG. 4. Comparison between experimental Rabi oscillation data (panel a) and simulations (rest of panels). (a) Rabi oscillation data. (b) Simulation, using optimal values of parameters: $\Delta_1/h = 2.7$ GHz, $\Delta_2/h = 3.5$ GHz, $\delta\epsilon = 45$ μeV and $\Gamma_\epsilon = 5.98$ GHz. (c) Simulation, using optimal parameters as in (b), but with only a single anticrossing (a two-state model). It is clear that a single anticrossing is insufficient to explain the data. Panels (d) and (e) are simulations with the optimal values of all the parameters as in (b), except for the anticrossing separation $\delta\epsilon$. In (d) and (e), $\delta\epsilon = 60$ μeV and 90 μeV , respectively. Comparing (b), (d) and (e), it is clear that as the detuning difference $\delta\epsilon$ between the first and the second anticrossings increases, the frequency of oscillations at far positive detuning increases as well. (f) Simulated data using optimal parameter values as in (b), but with the value of tunnel coupling at the second anticrossing being 1.5 times of the optimal: $\Delta_2/h = 5.25$ GHz. The main features of this simulation are qualitatively similar to (b), with the correct frequency of oscillations at large positive detuning, but with higher visibility.

charge states. Using Eq. (5), the detuning-dependent dephasing parameter Γ_ϵ is determined by experimentally extracted dephasing rates at two detuning values, namely the intrinsic dephasing rate $\Gamma_i = 0.48$ GHz at $\epsilon = 0$, and the T_2^* value of 179 ps at $\epsilon = -63$ μeV , which yields $\Gamma_\epsilon = 5.98$ GHz. Optimal values of the other parameters can then be found to give the best fit to the data. We found that the optimal values of the parameters that give the best fit to the data are: $\Delta_1/h = 2.7$ GHz, $\Delta_2/h = 3.5$ GHz, and $\delta\epsilon = 45$ μeV .

Here, we briefly explain how the parameters were obtained. The frequency of oscillation at the first anticrossing at $\epsilon = 0$ is very sensitive to the value of the first tunnel coupling and sets the value of Δ_1 , as is consistent with the usual Rabi dynamics of two-level systems. Because the pulse is not entirely abrupt, detuning pulses that reach beyond the first anticrossing (that is, to

$\epsilon > 0$) necessarily induce Landau-Zener-Stueckelberg interference effects [30–33]. For the energy level structure we study here, the presence and proximity of the second anticrossing to the first results in population of both G(1,2) and E(1,2), states $|b\rangle$ and $|c\rangle$. The frequency of oscillations at far positive detuning is strongly dependent on the anticrossing separation $\delta\epsilon$, and that frequency essentially fixes $\delta\epsilon$. In contrast, the tunnel coupling at the second anticrossing Δ_2 primarily affects the visibility of these oscillations.

Fig. 4 show a comparison of simulated data using various parameters. Panel (a) shows the experimental Rabi oscillation data (reproduced from Fig. 2(c) of the main text). Panel (b) shows the simulated data using the optimal parameters, displaying excellent agreement with the main features of the data shown in panel (a).

In order to ascertain whether the oscillations at far

positive detuning can be explained by having only one anticrossing, simulated data, shown in Panel (c), show the result for a two-state model with one anticrossing. This simulation with a single anticrossing shows clear discrepancies with the data at large positive detuning, even though there is a good match at zero detuning. It is clear that in order to consistently explain the data — especially the prominent nearly parallel lines at $\varepsilon > 0$ — a single anticrossing is insufficient.

The frequency of oscillations at far positive detuning is affected by the proximity of the second anticrossing to the first. Panels (d) and (e) are simulated data using all of the optimal values of the parameters, except for the anticrossing separation $\delta\varepsilon$. In panel (b), $\delta\varepsilon = 45 \mu\text{eV}$, while in panels (d) and (e) $\delta\varepsilon = 60 \mu\text{eV}$ and $90 \mu\text{eV}$ respectively. Comparing these panels, it is clear that the proximity of the second anticrossing plays an important role in determining the number of secondary oscillations at far positive detuning.

Finally, panel (f) shows simulated data using the optimal parameter values, but at 1.5 times the optimal tunnel coupling at the second anticrossing: $\Delta_2/h = 5.25 \text{ GHz}$. This data is qualitatively similar to the simulation using optimal parameters in (b), possessing the same number of oscillations at large positive detuning, but with higher visibility. We found, over a reasonably wide range of values, that Δ_2 affects mainly the visibility of the oscillations, and it has only a weak affect on the frequency of oscillations. This behavior is consistent with the interpretation of the oscillations arising from Landau-Zener-Stueckelberg interference.

[1] Y. Nakamura, Y. A. Pashkin, and J. S. Tsai, *Nature* **398**, 786 (1999).
[2] T. Yamamoto, Y. A. Pashkin, O. Astafiev, Y. Nakamura, and J. S. Tsai, *Nature* **425**, 941 (2003).
[3] T. Hayashi, T. Fujisawa, H. D. Cheong, Y. H. Jeong, and Y. Hirayama, *Phys. Rev. Lett.* **91**, 226804 (2003).
[4] K. D. Petersson, J. R. Petta, H. Lu, and A. C. Gossard, *Phys. Rev. Lett.* **105**, 246804 (2010).
[5] O. Astafiev, Y. Pashkin, Y. Nakamura, T. Yamamoto, and J. Tsai, *Phys. Rev. Lett.* **93**, 267007 (2004).
[6] C. Tahan, M. Friesen, and R. Joynt, *Phys. Rev. B* **66**, 035314 (2002).
[7] M. Prada, R. H. Blick, and R. Joynt, *Phys. Rev. B* **77**, 115438 (2008).
[8] L. V. C. Assali, H. M. Petrilli, R. B. Capaz, B. Koiller, X. Hu, and S. Das Sarma, *Phys. Rev. B* **83**, 165301 (2011).
[9] B. M. Maune, M. G. Borselli, B. Huang, T. D. Ladd, P. W. Deelman, K. S. Holabird, A. A. Kiselev, I. Alvarado-Rodriguez, R. S. Ross, A. E. Schmitz, M. Sokolich, C. A. Watson, M. F. Gyure, and A. T.

Hunter, *Nature* **481**, 344 (2012).
[10] J. R. Petta, A. C. Johnson, J. M. Taylor, E. A. Laird, A. Yacoby, M. D. Lukin, C. M. Marcus, M. P. Hanson, and A. C. Gossard, *Science* **309**, 2180 (2005).
[11] H. Bluhm, S. Foletti, I. Neder, M. Rudner, D. Mahalu, V. Umansky, and A. Yacoby, *Nat. Phys.* **7**, 109 (2011).
[12] M. D. Shulman, O. E. Dial, S. P. Harvey, H. Bluhm, V. Umansky, and A. Yacoby, *Science* **336**, 202 (2012).
[13] K. C. Nowack, F. H. L. Koppens, Y. V. Nazarov, and L. M. K. Vandersypen, *Science* **318**, 1430 (2007).
[14] D. Loss and D. P. DiVincenzo, *Phys. Rev. A* **57**, 120 (1998).
[15] B. E. Kane, *Nature* **393**, 133 (1998).
[16] R. Vrijen, E. Yablonovitch, K. Wang, H. Jiang, A. Balandín, V. Roychowdhury, T. Mor, and D. DiVincenzo, *Phys. Rev. A* **62**, 012306 (2000).
[17] D. P. DiVincenzo, D. Bacon, J. Kempe, G. Burkard, and K. B. Whaley, *Nature* **408**, 339 (2000).
[18] Z. Shi, C. B. Simmons, J. R. Prance, J. K. Gamble, T. S. Koh, Y.-P. Shim, X. Hu, D. E. Savage, M. G. Lagally, M. A. Eriksson, M. Friesen, and S. N. Coppersmith, *Phys. Rev. Lett.* **108**, 140503 (2012).
[19] T. S. Koh, J. K. Gamble, M. Friesen, M. A. Eriksson, and S. N. Coppersmith, “Pulse-gated quantum dot hybrid qubit,” Preprint arxiv:1207.5581.
[20] M. Thalakulam, C. B. Simmons, B. M. Rosemeyer, D. E. Savage, M. G. Lagally, M. Friesen, S. N. Coppersmith, and M. A. Eriksson, *Appl. Phys. Lett.* **96**, 183104 (2010).
[21] C. B. Simmons, J. R. Prance, B. J. Van Bael, T. S. Koh, Z. Shi, D. E. Savage, M. G. Lagally, R. Joynt, M. Friesen, S. N. Coppersmith, and M. A. Eriksson, *Phys. Rev. Lett.* **106**, 156804 (2011).
[22] Z. Shi, C. B. Simmons, J. Prance, J. K. Gamble, M. Friesen, D. E. Savage, M. G. Lagally, S. N. Coppersmith, and M. A. Eriksson, *Appl. Phys. Lett.* **99**, 233108 (2011).
[23] C. B. Simmons, M. Thalakulam, B. M. Rosemeyer, B. J. Van Bael, E. K. Sackmann, D. E. Savage, M. G. Lagally, R. Joynt, M. Friesen, S. N. Coppersmith, and M. A. Eriksson, *Nano Letters* **9**, 3234 (2009).
[24] D. Vion, A. Aassime, A. Cottet, P. Joyez, H. Potheir, C. Urbina, D. Esteve, and M. H. Devoret, *Science* **296**, 886 (2002).
[25] Y. Dovzhenko, J. Stehlik, K. D. Petersson, J. R. Petta, H. Lu, and A. C. Gossard, *Phys. Rev. B* **84**, 161302 (2011).
[26] J. K. Gamble, M. Friesen, S. N. Coppersmith, and X. Hu, *Phys. Rev. B* **86**, 035302 (2012).
[27] S. Harvey, M. Shulman, O. Dial, H. Bluhm, V. Umansky, and A. Yacoby, “Fast exchange oscillations in quantum dot spin qubits,” BAPS.2012.MAR.L29.8.
[28] M. A. Nielsen and I. L. Chuang, *Quantum Computation and Quantum Information* (Cambridge University Press, Cambridge, 2000).
[29] H.-P. Breuer and F. Petruccione, *The Theory of Open Quantum Systems* (Oxford Univ. Press, USA, 2002).
[30] L. D. Landau, *Phys. Z. Sowjetunion* **2**, 46 (1932).
[31] C. Zener, *Proc. R. Soc. London Ser. A* **137**, 696 (1932).
[32] E. Stückelberg, *Helv. Phys. Acta* **5**, 369 (1932).
[33] J. R. Petta, H. Lu, and A. C. Gossard, *Science* **327**, 669 (2010).